Available online at www.sciencedirect.com
SCIENCE DIRECT®
Journal of Structural Biology 144 (2003) 209–218
Journal of Structural Biology
www.elsevier.com/locate/yjsbi

Three-dimensional diffractive imaging for crystalline monolayers with one-dimensional compact support

J.C.H. Spence,[a,*] U. Weierstall,[a] T.T. Fricke,[b] R.M. Glaeser,[b] and K.H. Downing[c]

[a] *Department of Physics, Arizona State University, Tempe, AZ 85287-1504, USA*
[b] *Department of Molecular and Cell Biology, University of California, Berkeley, CA 94720, USA*
[c] *Life Sciences Division, Lawrence Berkeley National Laboratory, Berkeley, CA 94720, USA*

Received 16 June 2003, and in revised form 19 August 2003

Abstract

The use of a compact support constraint along the beam direction is considered as a solution to the phase problem for diffraction by two-dimensional protein crystals. Specifically we apply the iterative Gerchberg–Saxton–Fienup algorithm to simulated three-dimensional transmission electron diffraction data from monolayer organic crystals. We find that oversampling along the reciprocal-lattice rods (relrods) normal to the monolayer alone does not solve the phase problem in this geometry in general. However, based on simulations for a crystalline protein monolayer (lysozyme), we find that convergence is obtained in three dimensions if phases are supplied from a few high resolution electron microscope images recorded at small tilts to the beam direction. In the absence of noise, amplitude-weighted phase residuals of around 5°, and a cross-correlation coefficient of 0.96 between the true and estimated potential are obtained if phases are included from images at tilts of up to 15°. The performance is almost as good in the presence of noise at a level that is comparable to that commonly observed in electron crystallography of proteins. The method should greatly reduce the time and labor needed for data acquisition and analysis in cryo-electron microscopy of organic thin crystals by avoiding the need to record images at high tilt angles.

Keywords: Electron crystallography; Diffraction; Protein structure; Phase determination

1. Introduction

In recent work the idea has become widely accepted that the intensity scattered by a non-periodic object, if sampled finely enough, contains enough information to solve the phase problem. Several methods for extracting this information have been proposed involving the solution of the Fourier equations relating real and reciprocal space. The most successful of these is the iterative Gerchberg–Saxton–Fienup hybrid input–output (HIO) algorithm, referred to here as HIO (Fienup, 1982). The algorithm iterates between real and reciprocal space, imposing known information (constraints) in each space, until convergence is reached. Feedback is also used, making convergence more rapid and robust. For weakly scattering (real) objects the Fourier modulus, sign and compact support constraints have been found sufficient for convergence in simulations and experiments with X-rays (He et al., 2003; Miao et al., 1999), laser-light, and coherent electrons in TEM (Weierstall et al., 2001), where the first atomic-resolution images have recently been obtained from a nanotube, using diffracted intensities (Zuo et al., 2003). Simulations have also been reported for neutron imaging (Spence et al., 2001). The sign constraint here refers to the known sign of the scattering "potential" (charge-density for X-rays, electrostatic potential for electron scattering). Compact support refers to the requirement that the boundary of the object be approximately known. For "complex" objects (such as multiply-scattering samples in electron diffraction) inversion to the exit-face wavefunction is still possible, but requires very precise knowledge of the object boundary (support), and is facilitated if the support is disjoint (Fienup, 1987) or if the unit modulus constraint can be used for strong phase

* Corresponding author. Fax: 1-480-968-7954.
E-mail address: spence@asu.edu (J.C.H. Spence).

1047-8477/$ - see front matter © 2003 Elsevier Inc. All rights reserved.
doi:10.1016/j.jsb.2003.09.019

objects (Spence et al., 2002). Questions of the uniqueness of solutions, convergence, error metrics, relationship to steepest-descent optimizers (Fienup, 1982) and an illuminating analysis using the methods of projections onto convex sets are all considered elsewhere (Bauschke et al., 2002; Elser, 2003; Stark, 1987).

The Shannon sampling theorem shows that the continuous distribution of diffracted intensity from a single molecule of width W can be obtained at any angle by interpolation from sampled values of the intensity if the samples occur at an angular spacing proportional to $1/(2W)$ (in one dimension). This spacing is the reciprocal of the width $2W$ of the Fourier Transform of the diffracted intensity, which is the autocorrelation function of the molecule, and so plays the role of the "bandlimit" in Shannon's theory. All the information contained in the scattered intensity (usually enough to solve the phase problem) can only be extracted if this Shannon sampling is used (Sayre, 1952). Periodic repetition of the molecule on a lattice with spacing W, however, will generate Bragg peaks at twice this angular separation, and hence the Bragg intensities alone (without other a priori assumptions) do not contain enough information to solve the phase problem. Thus no way has been found to use the HIO algorithm to solve the phase problem for large three-dimensional crystals.

Shannon sampling of the diffracted intensity (at intervals of $1/2W$) has been referred to as "oversampling" (by a factor of two), and corresponds to Bragg sampling in the situation in which the molecule is surrounded by a border of material (such as a water jacket or vacuum) which has the effect of doubling the unit cell dimensions. The imposition of "known" zeros in this region in real space during iterations can be thought of as compensating for the lack of a corresponding amount of phase information in reciprocal space, since the result makes the number of Fourier equations just equal to the number of unknown phases. In this sense, Shannon sampling is needed to extract all information, including phases, from the diffracted intensity. The HIO algorithm is then capable of finding the very large number of adjustable parameters (one phase for each diffracted pixel) given the compact support constraint (known region of zero charge density surrounding the molecule). The algorithm is tolerant to noise in simulations, however it has proven difficult to make the isolated, "real" (single scattering) samples with approximately known support which are needed for experiments (He et al., 2003). Several approaches to the problem of estimating the support of an object from that of its autocorrelation function have been suggested (Fienup et al., 1982).

In this paper, we point out that for thin, laterally periodic slabs in the transmission diffraction geometry, the condition of compact support may be applied in the non-periodic direction z normal to the slab. We explore the consequences of this, using simulations, for the phase problem in electron diffraction and cryomicroscopy.

It is known that the HIO algorithm fails in general for three-dimensional crystals (Millane, 1993), fails also in one dimension (unless the support is disjoint (Stark, 1987)), converges for real finite objects in two dimensions, and converges best in three dimensions (Millane, 1990). The thin crystalline geometry we discuss here, periodic in two directions and non-periodic in the third, remains to be investigated. In surface science, a one-sided compact support condition has been applied normal to the termination of bulk material together with direct methods (Marks, 1999). We are especially interested in determining the minimum number of known phases which must be supplied from electron microscope images, perhaps at limited resolution, to phase the entire three-dimensional reciprocal space when the compact support condition can be applied along z. Since knowledge of phase is a convex constraint (Lindaas et al., 1998), these images greatly improve convergence. In this way, by requiring fewer images, the time and effort devoted to data collection and analysis in electron crystallography might be greatly reduced.

2. The HIO algorithm

We briefly summarize here the HIO algorithm (Fienup, 1982), which we will apply to three-dimensional diffraction data sets using three-dimensional Fourier iterations. For a monolayer potential $V(x,y,z)$, we assume that $|\mathrm{FT}(V(x,y,z))|$ has been measured, and that the support $S(x,y,z)$ is known. $S(x,y,z)$ is the region (slab) around $z=0$, where V is known to be non-zero. The iterations start with an initial estimate $\tilde{G}_1(u,v,w) = |\mathrm{FT}(V(x,y,z))|\exp(\mathrm{i}\theta_1(u,v,w))$ of the diffracted intensities. The zero-order Fourier coefficient or mean inner potential would need to be included in order to guarantee a known sign for the potential. However, we were interested to find here, that the algorithm works well without applying any sign constraint - evidently the provision of some known phases (a powerful convex constraint) compensates for the lack of a sign constraint in this work. Thus the mean potential was taken to be zero. Initially the phases $\theta_1(u,v,w)$ are random numbers in the range 0–2π. In the centrosymmetric case, phases are either 0 or π, so that the initial $\theta_1(u,v,w)$ correspond to an array of random + and − signs. The iterative HIO algorithm used here consists of the following steps (with subscript k labeling quantities at the kth iteration):

1. Inverse Fourier transform $\tilde{G}_k(u,v,w)$ to obtain an estimate of the potential $\tilde{g}_k(x,y,z)$.
2. Apply constraint to potential; the potential has to be real and positive: $\tilde{g}_k(x,y,z) = |\tilde{g}_k(x,y,z)|$. This condition was not applied in this work.
3. Define $g_{k+1}(x,y,z)$ as

$$g_{k+1}(x,y,z)=\begin{cases}\tilde{g}_k(x,y,z) & \text{if } (x,y,z)\in S(x,y,z),\\ g_k(x,y,z)-\beta\tilde{g}_k(x,y,z) & \text{if } (x,y,z)\notin S(x,y,z).\end{cases}$$

This constitutes the HIO version of the algorithm. β is a feedback constant chosen between 0.5 and 1. In the error-reduction (ER) version of the algorithm (the Gerchberg–Saxton algorithm) this step is replaced by

$$g_{k+1}(x,y,z)=\begin{cases}\tilde{g}_k(x,y,z) & \text{if } (x,y,z)\in S(x,y,z),\\ 0 & \text{if } (x,y,z)\notin S(x,y,z).\end{cases}$$

4. Fourier transform $g_{k+1}(x,y,z)$ to obtain $G_{k+1}(u,v,w)$.
5. Define new Fourier domain function $\tilde{G}_{k+1}(u,v,w)$ using the known Fourier modulus $|\mathrm{FT}(V(x,y,z))|$ with the computed phase: $\tilde{G}_{k+1}(u,v,w)=|\mathrm{FT}(V(x,y,z))|\exp(\mathrm{i}\theta_{k+1}(u,v,w))$.
6. Apply constraint to structure factors phases, which must be 0 or π, by replacing $\exp(\mathrm{i}\theta_{k+1}(u,v,w))$ with $\cos(\theta_{k+1}(u,v,w))/|\cos(\theta_{k+1}(u,v,w))|$. For acentric structures (such as the protein considered later) this step is omitted.
7. Replace any phases with values known from electron microscope images.

Go to step 1, with k replaced by $(k+1)$.

To monitor the progress of the algorithm, the image space error metric ε_k is calculated during each iteration:

$$\varepsilon_k=\left(\frac{\sum_{(x,y)\notin S}\left|\tilde{g}_k(x,y,z)\right|^2}{\sum_{(x,y)}\left|\tilde{g}_k(x,y,z)\right|^2}\right)^{1/2}. \quad (1)$$

Here ε_k is the amount by which the reconstructed potential violates the image-space constraints. It measures the deviation from the current estimate of the potential from zero outside the slab. (It has been shown that the likelihood of finding more that one solution of the correct sign which meets the condition $\varepsilon_k=0$, and possesses the correct Fourier magnitudes, is extremely small (Barakat and Newsam, 1984)).

The iterations used in this work consist of 25 HIO sequences followed by 10 error-reduction sequences, a combination found most effective during computational trials. The value of ε_k is only given accurately during error-reduction, whereas only during HIO iterations does feedback allow the algorithm to "climb out" of local minima.

3. Small molecules at atomic resolution: tetracyanoethelene

In order to establish the method using a recognizable atomic-resolution potential defined by few parameters, we first present the results of simulations for tetracyanoethelene (TCNE). Unlike the protein treated later, a glance at the retrieved three-dimensional potential gives an immediate impression of success or failure, the calculations are fast, and the results allow us to compare performance for centrosymmetric and noncentrosymmetric (acentric) molecules. Fig. 1 shows the structure of the TCNE crystalline monolayer used in the simulations. TCNE, C_6N_4, is body-centered cubic, with spacegroup Im3 and cell constant 9.736 Å (Belemlilga et al., 1999). The three inequivalent molecules per cell are shown in Fig. 1. A center of symmetry at (1/4,1/4,1/4) generates three more molecules that are arranged in a mutually perpendicular fashion. Using a Gaussian expansion for the relevant relativistic Hartree–Fock electron scattering factors (Doyle and Turner, 1968) we have simulated the kinematic diffraction pattern of amplitudes for a single layer of these molecules. We assume that the moduli of the Fourier coefficients of the electrostatic potential can be extracted from experimental diffraction patterns after correction for effects due to film bending, curvature of the Ewald sphere and other artifacts. A temperature factor $\exp(-B\mathbf{s}^2)$ with $B=0.3$ Å^2 and $\mathbf{s}=1/d_{hkl}$ was assumed. Since the molecule is centrosymmetric, the structure factors are real, and the phase problem consists of a sign ambiguity. Application of the HIO algorithm to solve this structure requires "oversampling" of the data along the relrods normal to the film, which are separated laterally by multiples of the Bragg angle. For a thin film of thickness t, the maximum sampling interval along the rod at the Shannon rate is $\Delta s=1/(2t)$, where Δs is a reciprocal lattice increment along the rod. (The sampling actually used in these simulations is discussed further below.)

To summarize, the magnitudes of the Fourier coefficients of potential for a TCNE monolayer were used as input to the HIO algorithm with the addition of a compact support condition normal to the slab. In practice a computational supercell was used whose

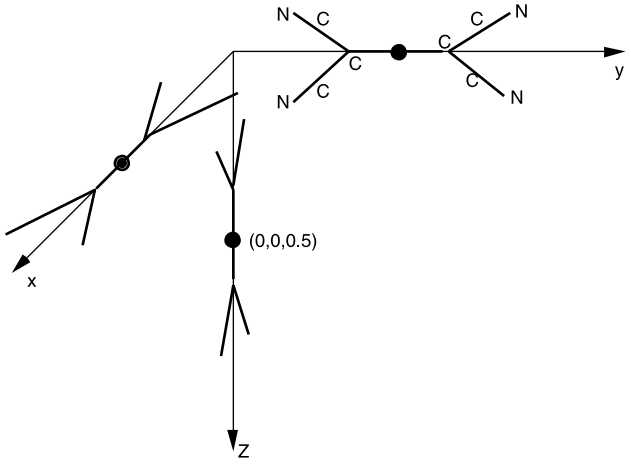

Fig. 1. Arrangement of molecules in the cubic unit cell of a tetracyanoethelene (TCNE) crystal. Additional molecules are generated by a center of inversion at (1/4,1/4,1/4). The center of inversion for the molecule lies at the midpoint of the cell axes.

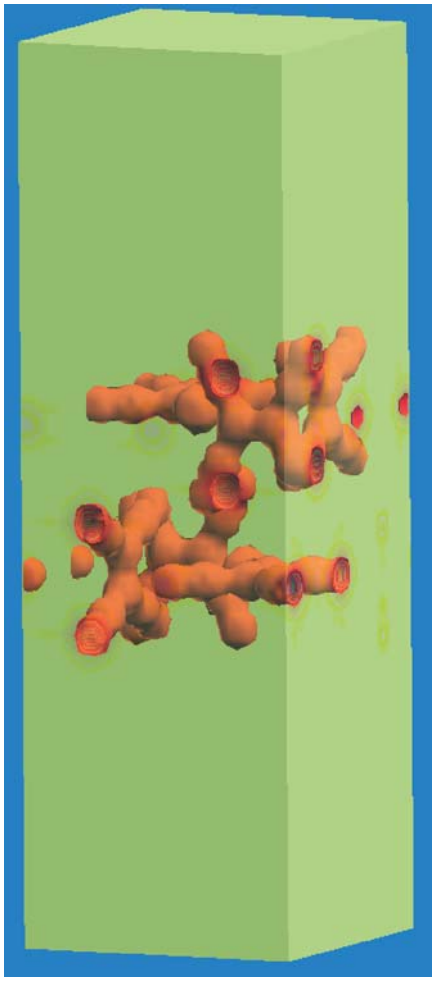

Fig. 2. Isopotential view of the electrostatic potential of TCNE as reconstructed by HIO from simulated diffracted intensities (to 0.35 Å) combined with 3 images (to 0.35 Å). The computational supercell is shown in green, the size in the z direction is three times the thickness of the monolayer, providing for the compact support. The size in the x and y direction is the size of one unit cell (0.97 nm). Seventy iterations were needed for the $30 \times 30 \times 90$ voxel data set.

dimensions were equal to the crystal monolayer unit cell dimension laterally, but three times this dimension measured along z, normal to the monolayer. This corresponds to an oversampling factor $N = 3$, which then fixes the points at which samples are taken along the relrods. While oversampling by 2 satisfies the Shannon requirement, it has been suggested in X-ray HIO work (Miao et al., 1999) that better convergence is obtained at somewhat higher factors.

If no additional phases were provided a priori, it was found that the HIO algorithm with compact support along z did not converge. We then assumed that phases can be provided from high resolution images recorded in various orientations. The algorithm was then found to converge after about 100 iterations (in the sense that a small value of ε_k is soon obtained and a recognizable charge-density obtained, as in Fig. 2) if three images were used to provide known phases. These were chosen on the plane in reciprocal space normal to c passing through the origin, together with planes tilted at 45° about the x and y axis. Fig. 2 shows an isopotential view of a contour of the electrostatic potential for the TCNE molecule. This was reconstructed after 70 iterations of the $30 \times 30 \times 90$ voxel data set with the feedback parameter $\beta = 0.8$. The simulated diffracted intensities (to 0.35 Å) were combined with phase data from a simulated image, also to 0.35 Å resolution. The support mask sets the object function to zero for slices equal to or less than 28 and greater than or equal to 62, corresponding to the vacuum before and after the sample. The algorithm converges to values of ε_κ of about 0.047 after only 70 iterations, independent of the starting phases. (In terms of the error metrics defined in the next section, after 105 iterations we find a correlation coefficient between the estimated and true charge density of $CC = 0.995$, $\varepsilon_\kappa = 0.047$). These calculations do not simulate the effects of noise.

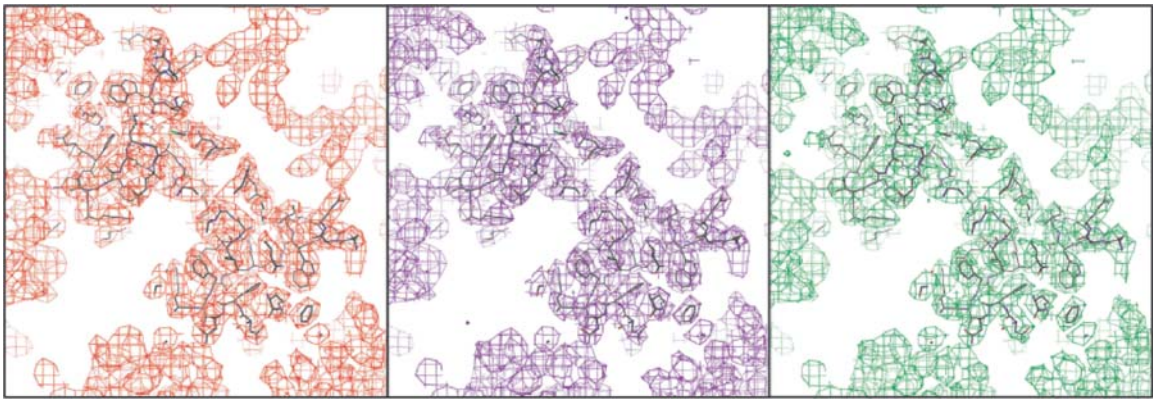

Fig. 3. A section of the unit cell of lysozyme normal to z, comparing model and retreived structures. Left: The model. Center: Reconstructed using HIO, with noise-free amplitudes and image phases up to 15° tilt angles; 105 iterations. Right: Similar reconstruction, with noise added to structure factors corresponding to $R = 25\%$ and using image phases up to 15° tilts.

4. Proteins at 3.0 Å resolution: lysozyme

More relevant to cryomicroscopy are applications of the method to proteins at the lowest resolution which allows identification of amino acids. We therefore consider the problem of phasing a three-dimensional diffraction data set from a crystalline monolayer of lysozyme. Atomic coordinates were obtained from the Protein Data Bank (ID 5LYZ (Diamond, 1974)). The unit cell is tetragonal, P 43 21 2 (#96), with cell constants $a = 79.1$ Å, $b = 79.1$ Å, $c = 37.9$ Å. Symmetry-related atoms were generated from the asymmetric unit to fill the unit cell (total of 8008 atoms), which was then padded to three times the initial size in the c direction to provide three times oversampling. Structure factors for this expanded cell were calculated with the CCP4 routine SFALL (Collaborative Computing project Number 4, 1994) using the electron scattering factor library. Structure-factor phases were randomized for this tripled structure, and the resulting intensities supplied to the HIO algorithm, which again performs three-dimensional Fourier iterations. A support mask was applied, set to unity within the monolayer slab and zero elsewhere. At 3 Å resolution these (tripled) cell dimensions require a matrix of dimension $54 \times 54 \times 78$. Running in Matlab 5.2 on a Mac G4 laptop, the program takes about one second per iteration, using FFT routines (not powers of two). Convergence could again only be obtained if known phases were supplied on certain planes in reciprocal space from images, but the algorithm is remarkably tolerant to noise in the amplitudes. Some results at 3 Å resolution are shown in Fig. 3.

Evaluation of the performance of the algorithm requires a statistical measure of the accuracy of the phasing of about 53 000 reflections. For these simulations, unlike experiment, the true (model) potential is known. We therefore evaluate several measures of convergence, and plot these under different conditions of noise, and of the number of images (and their orientations) used to assist the phasing.

The correlation coefficient between the true potential $V_t(\mathbf{r})$ and estimated potential $V_e(\mathbf{r})$ is equal to the value of the normalized cross-correlation function at the origin, or (Read, 1986)

$$\begin{aligned} \mathrm{CC} &= \frac{\int_V V_t(\mathbf{r}) V_e(\mathbf{r})\,\mathrm{d}\mathbf{r}}{\left[\int_V V_t(\mathbf{r})^2\,\mathrm{d}\mathbf{r} \int_V V_e(\mathbf{r})^2\,\mathrm{d}\mathbf{r}\right]^{1/2}} \\ &= \frac{\sum_h \left|F_{\mathbf{h}}^t\right|\left|F_h^e\right| \cos\left(\phi_h^t - \phi_h^e\right)}{\left[\sum_h |F_h^t|^2 \sum_h |F_h^e|^2\right]^{1/2}} \\ &= \frac{\sum_h |F_h|^2 \cos\left(\phi_h^t - \phi_h^e\right)}{\sum_h |F_h|^2}. \end{aligned} \tag{2}$$

Here F_h are the measured structure factors used in the HIO, which adjusts only phases. The value of CC lies in the range $\mathrm{CC} = -1$ (anticorrelated) to $\mathrm{CC} = 1$ (perfect agreement). We find CC values around 0.2 for an

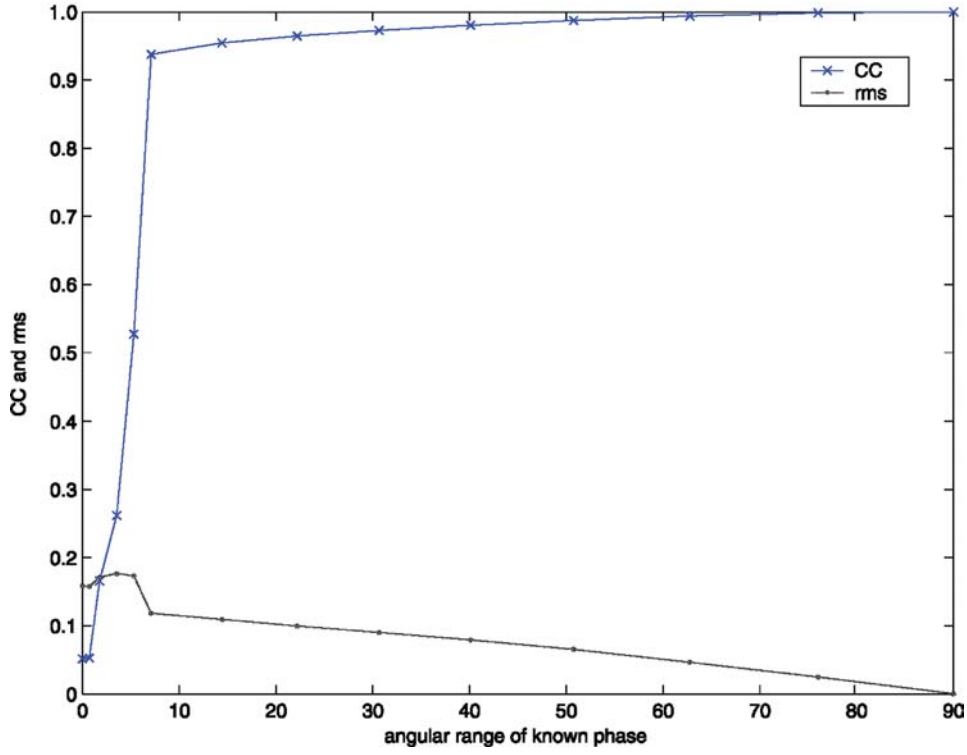

Fig. 6. Correlation coefficient CC (upper curve) and rms error (lower curve) from HIO algorithm plotted against the angular range of reciprocal space, in degrees, within which known phases have been supplied to the algorithm.

estimate based on the correct structure factor magnitudes and randomly selected phases, with one origin-fixing image. The value of CC depends on the average value of the potential, proportional to $F(000)$. (The addition of a large constant to two compact functions makes them more similar.) We therefore set $F(000) = 0$ when evaluating CC and the following phase residuals to avoid this effect and to increase the sensitivity of CC to differences. Because we set the zero-order Fourier coefficent $F(000)$ to zero the real-space potential fluctuates between positive and negative signs, and a sign constraint is therefore not used. The algorithm drives ε_κ (the total amount of potential outside the support) toward zero in order to find a solution. Setting $F(000) = 0$ sets a scale for ε_κ (and makes CC independent of $F(000)$), so that we can then use small values of ε_κ for an unknown sample as a predictor of large CC values. For two-dimensional image-processing applications of HIO with compact support it has been established that the variation of ε_κ with CC is monotonic (Fienup, 1997).

A useful measure of performance is the amplitude weighted rms phase error (Frank, 1996).

$$\langle|\langle\Delta\theta\rangle|\rangle_F = \left(\frac{\sum_h \left(\phi_h^{\mathrm{t}} - \phi_h^{\mathrm{e}}\right)^2 \left(|F_h^{\mathrm{t}}| + |F_h^{\mathrm{e}}|\right)}{\sum_h \left(|F_h^{\mathrm{t}}| + |F_h^{\mathrm{e}}|\right)}\right)^{1/2} = \mathrm{PRF}, \tag{3}$$

where ϕ_i^{t} are the N true structure factor phases from the model and ϕ_i^{e} are those estimated by the HIO algorithm, and the sums are taken over only the part of reciprocal space where the initial phases are unknown. In our case the structure factor amplitudes $|F_h^{\mathrm{t}}|$ and $|F_h^{\mathrm{e}}|$ remain equal during the HIO analysis.

A more informative measure is the resolution-dependent Fourier shell correlation (FSC):

$$\mathrm{FSC}(k, k+\Delta k) = \frac{\mathrm{Re}\sum_{[k,k+\Delta k]} F^{\mathrm{t}} F^{e^*}}{\left\{\sum_{[k,k+\Delta k]} F^{t\,2} \sum_{[k,k+\Delta k]} F^{e\,2}\right\}^{1/2}} \tag{4}$$

evaluated in the resolution range from k to $k + \Delta k$. (Frank, 1996).

Known phases, assumed supplied from electron micrographs, were provided on several planes passing through the origin of reciprocal space. In practice, one can expect to obtain a complete set of phases up to some angular limit from a number of images from crystals tilted at that angle but randomly oriented within the specimen plane. When the tilt angle is small, the number of images required to complete the phase set is also small. For example, with our lysozyme unit cell, all phases up to a 15° tilt could be obtained from images of about 15 crystals uniformly spaced in azimuth with respect to the tilt axis. Image resolution is assumed to be 3 Å, as for the diffraction patterns. In summary, in the absence of noise, a correlation coefficient of about 0.96 with PRF = 4.9° is obtained after about 100 iterations when phases up to 30° tilts are included. Convergence is essentially complete after 25 iterations, and CC and PRF improve little with further iterations. Results are almost as good with phases up to only 15° tilts. Fig. 3 shows a section of the density map obtained after 105 iterations with starting phases provided from images at tilt angles up to 15°. The map is indistinguishable from the initial model density map. Fig. 4 summarizes our results, showing CC and the RMS error ε_κ (the only metric available when analyzing unknown structures) as a function of iteration number.

The addition of noise to these simulated diffraction intensities provides a more realistic impression of results to be expected with real data. In these initial simulations we make the assumption that the noise follows Poisson statistics and ignore other sources of noise and error in the data. The standard deviation in the modulus of a structure factor $\sigma(|F_{\mathrm{g}}|)$ is then given by the square root of the number of (simulated) electrons that contribute to the measurement of $|F_{\mathrm{g}}|$. All structure factor amplitudes were scaled by the same factor to convert to electrons for each spot, and then each amplitude was replaced by a value taken from a normal distribution with the appropriate mean value for that diffraction spot. The scale factor was adjusted to obtain an R-factor, relating the noisy to noise-free amplitudes, that corresponds to values commonly found in experimental diffraction from proteins. As the noise level is increased, the number of iterations needed to reach a given value of the convergence parameter ε_κ increases. With sufficiently high noise, the algorithm stagnates with an unchanging value of ε_κ greater than about 0.1. With a noise level that produces an R-factor on amplitudes of 25%, the values of CC and PRF were only slightly worse than in the noise-free case, but convergence was about as fast. The final density map, as shown in Fig. 3, differs from the map in the noise-free case in merely minor ways that would not have any effect on its interpretation. (Here $R = \sum |F_{\mathrm{t}} - F_{\mathrm{n}}| / \sum F_{\mathrm{t}}$, with F_{t} and F_{n} the positive square root of the true and noisy intensities).

Fig. 4 also shows the effect of noise; the variation of CC and ε_k with iteration number is given for the two cases where starting phases are supplied at tilt angles up to 15° and 30°, respectively, with and without noise. An abrupt drop in the ε_κ curve occurs when the program changes from HIO to Error Reduction mode at iteration number 25, where 10 Error Reduction iterations are performed causing the error to fall significantly. When the HIO iterations start again there is generally a rapid increase in ε_κ to a plateau, along with a drop in CC. From Fig. 4 we see that ε_κ falls smoothly with the phase residuals as CC increases. Typically, CC rises from about 0.2 (random phases, correct structure factor magnitudes, some images) to 0.8 in the first few iterations, while ε_κ falls after a dozen iterations to values of less than 0.1. These limited computation trials therefore

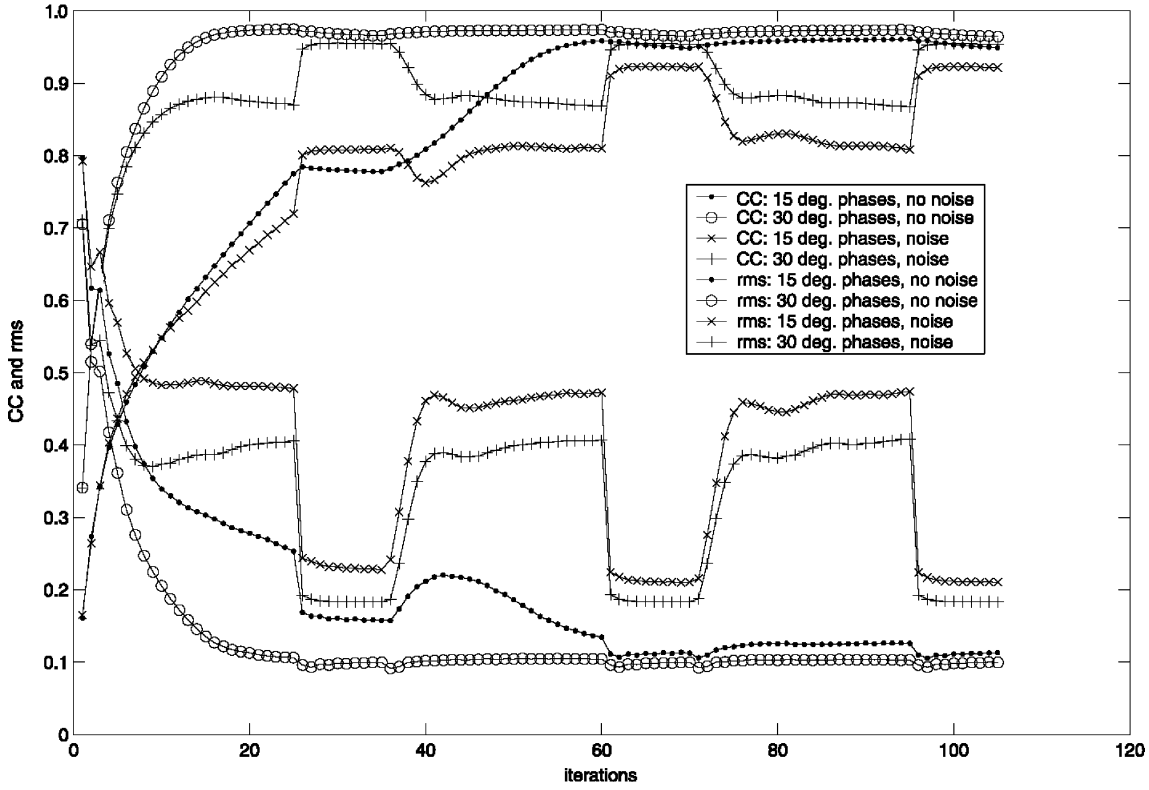

Fig. 4. Cross-correlation coefficient CC (upper curves) measuring agreement between model lysozyme potential and the HIO estimate as a function of iteration number. The error ε_k is also shown (lower curves). Calculations include starting phases as would be obtained from images at tilt angles up to 15 or 30°, with or without noise as shown in the key.

suggest that CC is again monotonic with ε_κ for our thin crystal geometry.

Fig. 5 shows the FSC for the four cases after 1, 35, 105, and 315 iterations. There is a slight falloff in the FSC at the higher resolution range, but even after the first series of HIO and ER iterations the FSC is already above the value of 0.5 generally taken to represent a reliable density map. We also note that the effects of noise and the limited range of starting phases are more pronounced at higher resolution.

In order to establish that ε_κ is a useful guide to the accuracy of reconstruction for unknown structures, it is also necessary to examine the dependence of ε_κ on the number of images used. Fig. 6 plots CC and ε_κ against the angular range within which the phases are known, corresponding to the maximum tilt angle for the images. The rapid decline of ε_κ with the angle is presumed to reflect the strong effect of incorporating even a small set of phase constraints.

It should be emphasized that the changes in ε_k and in the residuals and correlation coefficient due to variations in the random phasing used at the start of the algorithm are very small, typically 0.5% of ε_k. As in any experiment, systematic errors in data collection may result in convergence to the wrong solution. A full discussion of the extremely rare ambiguous solutions which may arise (whose complex Fourier Transforms are factorable), akin to the enantiomorphs which cannot be distinguished by HIO, can be found elsewhere (Seldin and Fienup, 1990). Equally rare homometric crystal structures (Buerger, 1959), those with entirely different structures but the same diffraction patterns, could not be distinguished by this algorithm.

5. Discussion

In this paper we have shown that repeated application of the boundary condition for a thin slab in an iterative algorithm can greatly assist solution of the phase problem for a two-dimensional crystal. Known phases are then only needed from images recorded over a small range of tilts in order to phase the entire reciprocal space volume, thus avoiding the need to record images at high tilt angles. The main advantage of the method presented here is the reduction in time and effort needed to complete a three-dimensional structural analysis, since image recording—especially at high tilts—is much more difficult than the recording of diffraction patterns. Although we need to sample the reciprocal lattice rods more finely, we only need to include more of the readily obtainable diffraction data. Thus there is some tradeoff in increasing the degree of oversampling to improve convergence versus increasing the number of diffraction

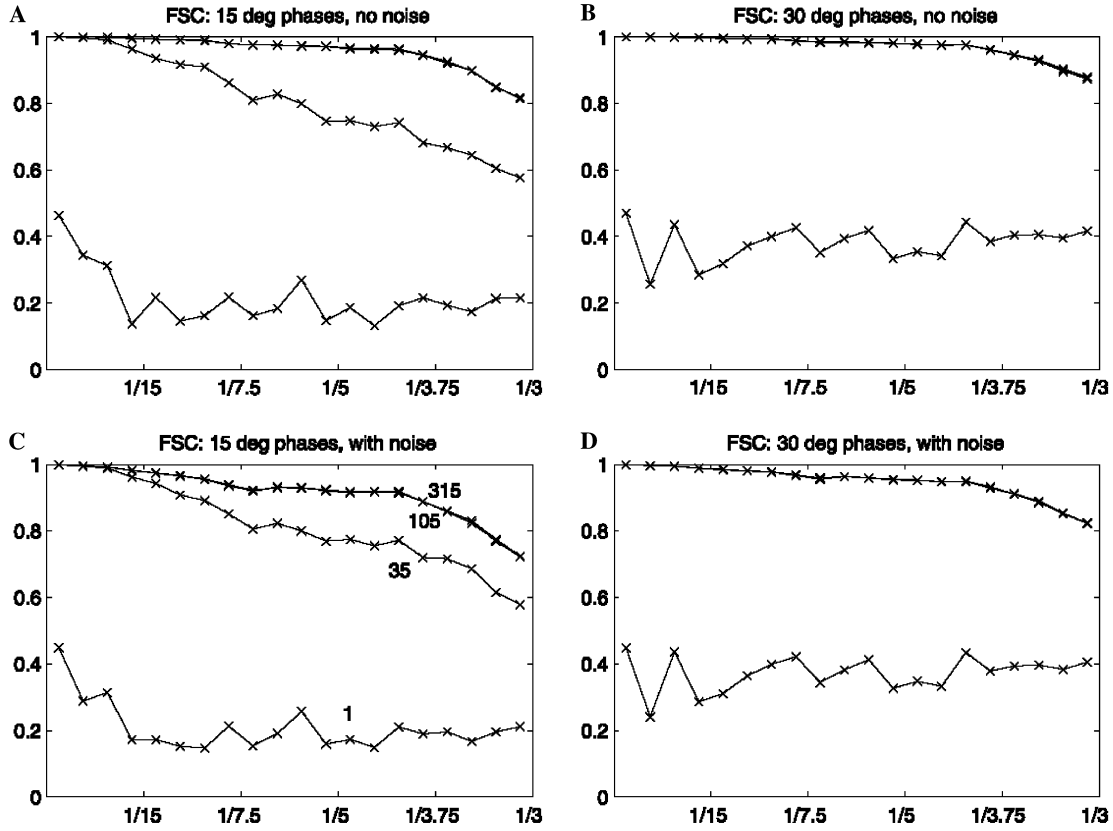

Fig. 5. Fourier shell correlation evaluated for the four simulations in Fig. 4 after 1, 35, 105, and 315 iterations as indicated in (C). In each case, convergence is essentially complete after 35 iterations when phases up to 30° tiltss are included, and after 105 iterations with only slightly lower FSC values when phases are only known up to 15°. The addition of noise to the amplitudes causes a slight drop in the correlation. The x-coordinate is resolution, in Å^{-1}.

patterns required. With 2× oversampling, in fact a similar number of data sets (images plus diffraction patterns) would be required as for the normal approach (Grigorieff et al., 1996; Nogales et al., 1998) but these would be all diffraction.

These simulations have made no use of the known space group symmetries of the infinite structure, which may be reduced to those of a slab for a monolayer. For lysozyme, with (422) point group, the structure factors are eightfold degenerate, in addition to the screw axis absences. (For (h00), $h = 2n$ and for (00l), $l = 4n$ are allowed.) Thus an optimized program might be written based solely on inequivalent reflections, in which the voxel number is then more than halved along each axis in both real and reciprocal space. This would increase the speed per iteration by a factor of about 20. The power of the support condition may also be applied laterally if some pixels of known "zero" potential can be applied within the unit cell. This method, akin to density modification or solvent flattening, would rapidly improve convergence.

The sensitivity of the method to errors in the estimate of the support dimension (the thickness of the sample) has been investigated. For TCNE, support width variations of several voxels were introduced until convergence was lost. We find that errors of up to 1.6 Å or 15% of the total thickness estimate can easily be tolerated without much effect on convergence, however this tolerance will depend on the noise in the data and use of the sign constraint. This parameter may also be refined during iterations, as in the recently developed "shrink-wrap" HIO algorithm for isolated objects, in which a support estimate based on the autocorrelation function is continuously improved during iterations (Marchesini et al., 2003).

Real experimental diffraction data includes both background and detector noise, which can seriously degrade the quality of weak reflections. To obtain an impression of this effect, the lysozyme simulations with 9 images (0, ±20 and ±30° tilts) were run with increased noise on weak reflections—those less than 5% of the maximum were subject to three times the standard deviation of the others. With $R = 18\%$, CC was found to decrease from 0.95 to 0.90 as a result, suggesting reasonable tolerance to this effect.

Errors in the phases obtained from images have also been investigated. If these are uniformly distributed over an interval of 60° (± 30°) or more, the algorithm fails to converge if 9 images are used up to 30° tilt. With noise on structure factor magnitudes corresponding to $R = 18\%$, the introduction of image phase errors

uniformly distributed over 45° causes a decrease in the nine-image case from CC = 0.95 to 0.93. There is a dramatic improvement in performance once the phase error becomes less than about 30° (± 15°). Experimental errors in phase determination from images are smaller than these limits at low resolution, but comparable at high resolution, suggesting that these conditions may be demanding for image phasing at high resolution—more images and a tighter support may help.

These reconstructions take no account of the "missing cone" of diffraction intensities present in experimental data, which generate an anisotropic point spread function in real space. Experience with the HIO algorithm in soft X-ray diffraction (He et al., 2003), where missing data arises from use of a beam-stop, shows that this can be dealt with by floating numerical values within the missing region (i.e. treating them as adjustable parameters). Setting aside any effort to fill in the missing cone, the anisotropic point spread function caused by the missing cone will be identical whether the phases are obtained by direct imaging or by diffraction imaging. Whether the degraded resolution in the z-dimension will interfere with setting a sufficiently accurate boundary for the compact support, such that diffraction phasing is successful, remains still to be investigated.

The domain of convergence for our approach has not been fully explored in this paper. The relationship between ε_κ, CC and the phase residuals might also be more fully explored for different structures and noise conditions. A modest "phase extension" effect was found in the simulation for tetracyanoethelyne, but the use of HIO to improve the resolution of images using higher-resolution diffraction data has not been fully explored here. For acentric thin crystals such as lysozyme, simulations showed that little can be gained—the 3 Å diffraction data could be phased using a set of images limited to 4 Å resolution, however CC fell to 0.90 and the algorithm stagnates at much lower resolution. It seems reasonable to expect that the convergence conditions should not depend on the particular protein, however this remains to be shown.

Acknowledgments

This work has been supported by ARO award DAAD190010500 and by NIH grant GM51487. We are most grateful to Drs. J. Plevert, R. Blessing, D. Langs, and J. Fienup for useful discussions.

References

Barakat, R., Newsam, G., 1984. Necessary conditions for a unique solution to two-dimensional phase recovery. J. Math. Phys. 25, 3190–3193.

Bauschke, H.H., Combettes, P.L., Luke, D.R., 2002. Phase retrieval, error reduction algorithm, and Fienup variants: a view from convex optimization. J. Opt. Soc. Am. 19, 1334.

Belemlilga, D., Gillet, J.M., Becker, P.J., 1999. Charge and momentum densities of cubic tetracyanoethylene and its insertion compounds. Acta Cryst. B 55, 192.

Buerger, M.J., 1959. Vector Space, and its Application in Crystal–Structure Investigation. New York, Wiley.

Collaborative Computing project Number 4, 1994. The CCP4 Suite: Programs for protein crystallography. Acta Cryst. D 50, 760–763.

Diamond, R.J., 1974. Real-space refinement of structure of hen egg-white lysozyme. J. Mol. Biol. 82, 371.

Doyle, P.A., Turner, P.S., 1968. Relativistic Hartree–Fock X-ray and electron scattering factors. Acta Cryst. A 24, 390.

Elser, V., 2003. Phase retrieval by iterated projections. J. Opt. Soc. Am. 20, 40–55.

Fienup, J.R., 1982. Phase retrieval algorithms: a comparison. Appl. Opt. 21, 2758–2769.

Fienup, R., 1987. Reconstruction of a complex-valued object from the modulus of its Fourier-transform using a support constraint. J. Opt. Soc. Am. A 4, 118–123.

Fienup, J.R., Crimmins, T.R., Holsztynski, W., 1982. Reconstruction of the support of an object from the support of its auto-correlation. J. Opt. Soc. Am. 72, 610–624.

Fienup, J.R., 1997. Invariant error metrics for image reconstruction. Appl. Opt. 36, 8352–8357.

Frank, J., 1996. Three-Dimensional Electron Microscopy of Macromolecular Assemblies. Academic Press, San Diego.

Grigorieff, N., Ceska, T., Downing, K.H., Baldwin, J., Henderson, R., 1996. Electron-crystallographic refinement of the structure of Bacteriorhodopsin. J. Mol. Biol. 259, 393.

He, H., Marchesini, S., Howells, M., Weierstall, U., Chapman, H., Hau-Riege, S., Noy, A., Spence, J.C.H., 2003. Inversion of X-ray diffuse scattering to images using prepared objects. Phys. Rev. B 67, 174114, See also He, H. et al., 2003. Experimental lensless soft-X-ray imaging using iterative algorithms: phasing diffuse scattering. Acta Cryst. A 59, 143.

Lindaas, S., Calef, B., Downing, K., Howells, M., Magowan, C., Pinkas, D., Jacobsen, C., 1998. X-ray holography of fast-frozen hydrated biological samples. In: Thieme, J. (Ed.), X-ray Microscopy and Spectromicroscopy. Springer, Berlin, p. II-75.

Marchesini, S., He, H., Chapman, H., Hau-Riege, S., Noy, A., Howells, M., Weierstall, U., Spence, J., 2003. Imaging without lenses. Phys. Rev. B., in press.

Marks, L.D., 1999. General solution for three-dimensional surface structures using direct methods. Phys. Rev. B 60, 2771.

Miao, J., Charalambous, P., Kirz, J., Sayre, D., 1999. Extending the methodology of X-ray crystallography for imaging of micrometre-sized non-crystalline specimens. Nature 400, 342.

Millane, R.., 1990. Phase retrieval in crystallography and optics. J. Opt. Soc. Am. 7, 394.

Millane, R.P.J., 1993. Phase problems for periodic images—effects of support and symmetry. J. Opt. Soc. Am. A 10, 1037, See also Millane, R.P., Stroud, W.J., 1997. Reconstructing symmetric images from their undersampled Fourier intensities. J. Opt. Soc. Am. A 14, 568; for use of non-crystallographic symmetry to assist phasing by HIO for macromolecular crystals.

Nogales, E., Wolf, S.G., Downing, K., 1998. The structure of alpha-beta tubulin dimer by electron crystallography. Nature 391, 199.

Read, R.J., 1986. Improved Fourier coefficients for maps using phases from partial structures with errors. Acta Cryst. A 42, 140–149.

Sayre, D., 1952. Some implications of a theorem due to Shannon. Acta Cryst. 5, 843.

Seldin, J.H., Fienup, J.R., 1990. Numerical investigation of the uniqueness of phase retrieval. J. Opt. Soc. Am. A 7, 412.

Spence, J., Weierstall, U., Friis, J., 2001. On lensless imaging of organics with neutrons X-rays, helium atoms and low energy

electrons: damage and iterative phase retrival. Microsc. Microanal. 7 (Suppl. 2), p. Proc. MSA.

Spence, J.C.H., Weierstall, U., Howells, M., 2002. Phase recovery and lensless imaging by iterative methods in optical X-ray, and electron diffraction. Phil. Trans. 360, 875.

Stark, H., 1987. Image Recovery: Theory and Applications. Academic Press, New York.

Weierstall, U., Chen, Q., Spence, J., Howells, M., Isaacson, M., Panepucci, R., 2001. Image reconstruction from electron and X-ray diffraction patterns using iterative algorithms: experiment and simulation. Ultramics 90, 171.

Zuo, J.M., Vartanyants, I., Gao, M., Zhang, R., Nagahara, L.A., 2003. Atomic resolution imaging of a carbon nanotube from diffraction intensities. Science 300, 1419–1421.